Optimal Site for Proximal Optimization Technique in Complex Coronary Bifurcation Stenting: A Computational Fluid Dynamics Study

Accepted manuscript at https://doi.org/10.1016/j.carrev.2019.12.015

Optimal Site for Proximal Optimization Technique in Coronary Bifurcation Stenting: a Computational Fluid Dynamics Study

Running Title: Proximal Optimization technique in Left Main bifurcation

Marco Zuin[1 *], Gianluca Rigatelli[2 *], Claudio Chiastra[3]

1 Section of Internal and Cardiopulmonary Medicine, University of Ferrara, Faculty of Medicine Ferrara, Italy; Division of Cardiology Santa Maria della Misericordia Hospital, Rovigo, Italy

2 Department of Cardiovascular Diagnosis and Endoluminal Interventions, Santa Maria della Misericordia Hospital, Rovigo, Italy.

3 PoliTo[BIO]Med Lab, Department of Mechanical and Aerospace Engineering, Politecnico di Torino, Turin, Italy

*The authors equally contribute to the manuscript

Type of Article: Original research

Conflict of interest: None of the authors have conflict of interest to declare

Key words: Left main; bifurcation; Myocardial infarction; Wall shear stress

For Correspondence:

Prof. Gianluca Rigatelli MD, FACP, FACC, FESC, FSCAI

Cardiovascular Diagnosis and Endoluminal Interventions,

Rovigo General Hospital, Viale Tre Martiri, 45100, Rovigo, Italy

Phone: +3903471912016; Fax: +390425394513;

e-mail: jackyheart@libero.it

Abstract

Background/purpose

The optimal position of the balloon distal radio-opaque marker during the post optimization technique (POT) remains debated. We analyzed three potential different balloon positions for the final POT in two different two-stenting techniques, to compare the hemodynamic effects in terms of wall shear stress (WSS) in patients with complex left main (LM) coronary bifurcation.

Methods/materials

We reconstructed the patient-specific coronary bifurcation anatomy using the coronary computed tomography angiography (CCTA) data of 8 consecutive patients (6 males, mean age 68.2± 18.6 years) affected by complex LM bifurcation disease. Subsequently a virtual bench test was performed in each patient using two different double stenting techniques represented by the DK and Nano crush using the reconstruction of Orsiro stents (Biotronik IC, Bulack, Switzerland).

Results

A significant reduction in the mean WSS values in all the lesion's sites was observed when the final POT was performed 1 mm distally the carina cut plane in both techniques. Moreover, a significant improvement in the mean WSS values of the entire SB (e.g. LCX) was obtained performing the POT 1 mm distally to the carina cut plane. The proximal POT resulted in larger area of lower WSS values at the carina using both the Nano crush and the DK crush techniques.

Conclusions

In patients with complex LM bifurcation disease the use of a final POT performed 1 mm distally to the carina cut plane might results in more favourable WSS patterns (i.e. higher WSS values) along all stented segments and, especially, along the entire LCX lesions.

1. Introduction

Over the latest years, both bench and computational analyses have suggested that proximal optimization technique (POT) offers some clear biomechanical advantages compared to the kissing balloon dilatation (KBD) during stenting of coronary artery bifurcation disease [[1], [2], [3], [4], [5]]. Currently, the POT is recommended by the European Bifurcation Club consensus paper [6] since this technique can correct both the proximal main vessel (MV) malapposition and side branch (SB) obstruction facilitating at the same time the SB re-wiring [7]. Generally, the POT is performed positioning the distal balloon marker just at the carina cut plain [6]. However, the optimal position of the balloon distal radio-opaque marker, with respect to the carina, remains debated.

As well known, wall shear stress (WSS) has a pivotal role in coronary arteries, exerting its effect on plaque progression, vascular remodeling, and arterial healing after percutaneous coronary intervention (PCI) [8]. In the present study, by using virtual bench stenting and computational fluid dynamics (CFD) analysis, we analyzed three potential different balloon positions for the final POT in two different two-stenting techniques, represented by the Nano and Double Kissing (DK) crush in the effort to compare the hemodynamic effects in terms of WSS in patients with complex coronary bifurcation.

2. Material and methods

2.1. Patient selection

We reconstructed the patient-specific coronary bifurcation anatomy using the coronary computed tomography angiography (CCTA) data of 8 consecutive patients (6 males, mean age 68.2± 18.6 years) affected by complex left main (LM) bifurcation disease evaluated between 1st January 2018 and 1st June 2018 at the section of Cardiovascular diagnosis and endoluminal interventions of Rovigo General Hospital, Italy.

Inclusion criteria were patients aged ≥18 years old with severe unprotected LM bifurcation disease assessed by both CCTA and then by coronary angiography (CA). Specifically, unprotected complex LM bifurcation disease was defined as: (1) a stenosis with a diameter of >50% involving the mid-shaft/distal main vessel with significant involvement (>50% luminal narrowing and >10 mm length by visual estimation) of the left anterior descending coronary artery (LAD) and left circumflex artery ostia (diameter > 2.5 mm by visual estimation) and, (2) without any patent graft to the left anterior descending artery or left circumflex artery.

Exclusion criteria were previous CABG, diffuse coronary artery disease or any significant (≤50% luminal narrowing) stenoses of LAD, LCX or right coronary artery (RCA) because any other focal narrowing or diffuse coronary disease might have produced some bias in the CFD analysis. Written informed consent for the CCTA and CA were obtained from all patients and the local Board approved the study.

2.2. Coronary computed tomography angiography

CCTA was acquired using a 64-slice multi-detector computed tomography scanner (64-detector row Lightspeed VCT scanner, GE Healthcare, Milwaukee, WI, USA). Per our institution protocol, before the imaging acquisition, patients were pre-treated with oral and/or intravenous beta-blockers, as necessary, to achieve a target resting heart rate (HR) < 70 beats/min. Electrocardiographic (ECG) gating was used for all scans. The scanning protocol was adjusted for patient weight and heart rate (HR). Blood pressure was measured with an arm-band sphygmomanometer just before the examination. A bolus intravenous dose of iodine contrast was given through the basilic or cephalic vein. The entire volume of the heart was acquired in 8–9 s during a single breath-hold. Each examination was independently interpreted by a trained CT radiologist using a combination of axial images, 3D volume-rendered images, multiplanar reformations, and maximum intensity projections [9].

2.3. Coronary angiography

CA was performed using a 6F radial approach. Angiographic data were reviewed by a 20 years-experienced angiographic operator (G.R.). Discordances between CCTA and CA results were resolved via collegial discussion with the CT radiologist. Quantitative coronary angiography (QCA) estimation (CAAS II 5.0 version; Pie Medical, Maastricht, The Netherlands) was used to quantify the coronary artery disease on CA while the type of bifurcation lesion was defined according to the Medina classification [10].

2.4. Coronary bifurcation model

Population-based models of complex LM bifurcation were created. The mean carina angle aw 72.3 ± 18.6°. All the bifurcation lesion were angiographically classified as Medina class 1,1,1 [10]. The stenoses involving the LM, LAD and LCX ostia were 84.2 ± 8.6%, 86.7 ± 3.1% and 83.2 ± 5.2%, respectively. The mean lesion lengths as well as basal and post-stenting mean lumen diameters (MLDs) are described in Table 1. The reconstructed vessel wall consisted of three layers

with realistic material properties of the coronary artery [11] while the atherosclerotic plaques were modelled as lipid with a 4 mm long half-calcified ring distal to the carina. Fibrous and calcium material properties were taken from experimental tests on human atherosclerotic tissues [12], while the lipid was modelled as a very soft material [13]. The coronary vessel and plaque meshes were composed by 6624 and 1843 elements, respectively.

2.5. Virtual bench stenting

Finite element analyses were performed to virtually deploy and post-dilate stents and balloons. We assumed that after stent deployment and implantation, both in the MB and SBs, there was no residual stenosis. The simulated coronary stent resembles the strut design and linkage pattern of the Orsiro stent (Biotronik IC, Bulack, Switzerland) and was generated by reverse-engineering using high-resolution micro-computed tomography imaging. The Orsiro stent is characterized by very ultrathin struts (60 μm up to 3.0 mm diameter stent and 80 mm up to 4.0 mm stent) [14]. To keep the analysis runtime reasonable, a finite element mesh consisting of 17,280 elements was used for the Orsiro stent. Moreover, since this device is made of a Co—Cr alloy, its material properties were taken from Schmidt et al. [15]. After the "virtual implantation" of the solid stent model in the proper position inside the bifurcation geometry, by using Boolean operation, the deployed stent, after the final POT was subtracted from the bifurcation to show the different distribution of WSS along the domain.

We applied two double stenting techniques: (1) the DK crush, representative of double stenting techniques with heavy metal amount at the carina, such as the classical crushing and the culotte technique, and (2) the nano-crush technique, representative of techniques with no or very low amount of metal at carina, such as the cross-over provisional T stent or mini crush.

2.6. Nano-crush

The technique was virtually replicated according to the following steps [16]: (1) Predilation of both branches; (2) Stenting of the LCx with a cell protrusion between 0.5 and 1 mm in the proximal LM; (3) Crushing of the stent with non-compliant balloon (NCB) in LM with a 1:1 ratio to LM diameter at 20 atm; (4) LM stenting; (5) POT with a NCB on a 1:1 balloon: vessel ratio to LM at 20 atm; (6) LCx rewiring; (7) Snuggle kissing with a NCB on a 1:1 balloon:vessel ratio; and (8) Final POT. An example of the stent geometry at the end of the procedure is showed in Fig. 1, Panel A.

2.7. Double kissing crush

The double kissing crush was virtually performed as follows [17]: 1) Predilation of both branches; 2) LCx stenting with protrusion into the LM; 3) Crush by LM dilation with NCB (20 atm); 4) Proximal LCx rewiring; 5) First KB 1:1 NCB; 6) LM stenting; 7) LCx dilation; and 8) Final kissing balloon. An example of stent geometry at the end of the analysis is showed in Fig. 1, Panel B.

2.8. Virtual final post optimization techniques

For the simulation we replicated and validated, according to the manufacturer's compliance chart a 4.0 × 12. Non-compliant Sprinter balloon (Medtronic, USA). Specifically, the balloon-tipped catheter consisted of a guide wire, a catheter shaft and a folded NCB. The guide wire and catheter shaft were discretised using 780 and 12,265 continuum elements, respectively, while the NC balloon was discretised using 13,578 membrane elements. In order to identify an appropriate mesh density, first a preliminary convergence study was carried out. The radio-opaque markers were reconstructed as well to ensure an adequate position of the marker for the final POT. The balloon material model was a classical one based on Hooke's theory of elasticity with Young's modulus $E = 900$ MPa and Poisson's ratio $\nu = 0.3$ [18,19].

Specifically, in each procedure, the POT was performed to the virtual distal shoulder position (balloon parallelism loss) relative to the carina cut plane (Fig. 2) and defined as follows:

- Proximal, when the distal marker was 1 mm before the carina
- Standard, when the distal marker was just at the carina cut plane
- Distal, when the distal marker was 1 mm after the carina.

2.9. Computational fluid dynamics models

The reconstruction methodology was based on three steps: image acquisition, segmentation and meshing. Specifically, to obtain the computational fluid domain, patient-specific geometries were reconstructed using the open-source software package VMTK (Vascular Modeling Toolkit, http://www.vmtk.org), identifying the MV vessel centerline and then splitting the branches of the bifurcation. In a second step, external wall surfaces were created with circumferential cross sections perpendicular to the center-lines using the computed-aided design software Rhinoceros 4.0 Evaluation (McNeel & Associates, Indianapolis, IN, USA) [20]. Atherosclerotic plaques were modelled considering the distance between each node and the centerline of the luminal surface. Coronary artery stenosis (Diameter Stenosis %) and minimal lumen area were calculated considering the reconstructed coronary artery model. Specifically, the severity of the stenosis was

computed as 100% minus the percentage of minimal lumen area to the reference lumen area. Subsequently, the patient-specific geometries were discretized using ICEM CFD (ANSYS Inc., Canonsburg, PA, USA) into tetrahedral volume elements with a maximum size of 0.2 mm [21]. Meshing parameters included also a maximum surface element size of 0.2 mm for the LM segment and 0.15 mm for the proximal length of both LAD and LCX (defined as the first tertile of the branch lengths) and carina, respectively. Moreover, a prism layer consisting of four layers with a height ratio of 1.2 was employed to capture the flow close to the lumen. A mesh independence analysis was performed before the CFD simulations using the region adaptation function in Fluent (ANSYS Inc.) to refine the computational grid.

Steady-state CFD simulations were performed using the commercial software Fluent (ANSYS Inc.) to solve the governing equations of fluid motion:

$$\rho v \cdot \nabla v = -\nabla \cdot \tau - \nabla P \quad (1)$$

$$\nabla \cdot v = 0 \quad (2)$$

where **v** is the 3D velocity vector, P pressure, ρ density and **τ** the viscous stress tensor.

The blood was modelled as a non-Newtonian and incompressible fluid with a density of 1060 kg/m^3 [[22], [23], [24], [25]]. In particular, the Casson model was chosen to describe the non-Newtonian fluid [24,25]. The boundary conditions used for the simulation were obtained from patient-specific data. Indeed, for the steady-state simulation, a constant velocity was applied at the inlet while a flow division at the outlet. In particular, to estimate the patient-specific flow-rate, the patient-specific stroke volume was calculated from the difference between the end-diastolic (EDV) and end-systolic volumes (ESV) and then combined with the measured heart rate (HR) to obtain their mean flow-rate. The calculated velocity was applied as inlet boundary condition at the LM entrance with a flat profile while a flow split was imposed at the two outlet boundaries represented by the end of LAD and LCX. Specifically, the Murray's law, which states that the flow division over two branches equals the ratio of the diameters to the power of 3 [26], was used to estimate the flow-split for the side branches.

2.10. Segmental analysis

The LM, LAD and LCX were divided into three sections, defined as proximal, medial and distal thirds. More precisely, the LM proximal thirds started with the beginning of the stenosis involving

the LM while the distal thirds ended in correspondence of the intersection of a virtual plane perpendicular to the LM longitudinal axis and another plan crossing the carina perpendicularly. Conversely, the proximal thirds of both LAD and LCX lesions started in correspondence of a virtual plane crossing the carina and perpendicular to the longitudinal axes of each vessel while the distal thirds ended with the end of each lesions, respectively. The medial thirds of each vessel's stenosis were calculated as consequence after setting the proximal and distal thirds (Fig. 3). The WSS was defined as the tangential force per unit of lumen area (Pa) that is tangentially acting to the surface due to friction [23]. In particular, the mean WSS, before and after final POT, was calculated at the proximal (WSS_{prox}), medial (WSS_{med}) and distal (WSS_{dist}) thirds at each branch of all stenotic vessels. Moreover, the mean WSS of the entire stenoses of each vessel, represented by the LM (WSS LM_{entire_lesion}), LAD (WSS LAD_{entire_lesion}) and LCX (WSS LCX_{entire_lesion}), were computed. Additionally, the mean WSS of the entire bifurcation (WWS_{entire_model}) was calculated.

2.11. Study endpoint

The study endpoint was to assess the differences in the mean regional WSS after performing the final POT in three different positions in patients with complex LM bifurcation disease virtually implanted using the Nano crush and DK crush techniques.

2.12. Statistical analysis

Continues variables were expressed as mean ± standard deviation (SD) and were compared by Student *t*-test if the data had normal distribution, otherwise by Wilcoxon-Mann-Whitney *U* test. Differences in the mean WSS among the three different POT positions were evaluated with ANOVA. Categorical variables presented as proportions and compared by the Pearson's χ^2 test. Statistical significance was defined as $p < 0.05$. Statistical analyses were performed using SPSS package version 20.0 (SPSS, Chicago, IL, USA).

3. Results

3.1. Lesion characteristics

The characteristics of the coronary artery lesions as well as the carina angle, derived from the baseline CA in the 8 consecutive patients reviewed (6 males, mean age 68.2 ± 18.6 years) to reconstruct the 3D models, baseline and after stenting MLDs as well as lesions lengths are showed in Table 1.

3.2. Wall shear stress analysis

The mean proximal, medial and distal WSS in each vessel and at each site significantly decrease using the three different POT positions (e.g distal, standard and proximal) (ANOVA $p < 0.001$) (Table 2). Specifically, the normal-higher mean WSS values were observed in each stented segment when the final virtual POT was performed positioning the distal marker of the balloon 1 mm distal to the carina cut plane. Intriguingly, the same favorable mean WSS values were confirmed independently from the stenting technique used for the simulation. Moreover, no significant differences in the mean WSS values were observed comparing the different lesions segments among the two stenting techniques in patients treated with the same type of POT.

While the use of a proximal POT generated low WSS values in all vessels and segments, independently from the stenting technique used, significant differences were observed comparing the standard POT (performed at the carina cut plane) with the distal POT in both the stenting techniques.

- *Standard* vs *Distal POT in Nano crush*: Significant higher WSS mean values were observed in the proximal and distal LM segments (6.2 ± 0.2 vs 5.4 ± 0.6 Pa, $p = 0.003$ and 6.5 ± 0.2 vs 5.8 ± 0.5 Pa, $p = 0.002$, respectively) and in the entire LCX lesion (6.1 ± 0.1 vs 5.2 ± 0.8 Pa, $p = 0.007$ and 6.1 ± 0.2 vs 5.5 ± 0.7 Pa, $p = 0.003$, respectively) (Table 2).
- *Standard* vs *Distal POT in DK crush*: The mean WSS values resulted improved (i.e. were higher) in the LM proximal segment comparing the standard and distal POT techniques in the DK crush simulation (6.1 ± 0.3 vs 5.6 ± 0.4 Pa, $p = 0.01$). Moreover, a significant improvement in WSS was observed in the distal LM segment (6.2 ± 0.6 vs 5.6 ± 0.5 Pa, $p = 0.04$) as well as in the distal and entire LCX lesion (6.2 ± 0.4 vs 5.3 ± 0.5 Pa, $p = 0.003$ and 6.2 ± 0.6 vs 5.6 ± 0.3 Pa, $p = 0.02$) (Table 2).
- *WSS at the carina*: The proximal POT resulted in larger area of lower WSS values at the carina using both the Nano crush and the DK crush techniques (Fig. 4, Panels A and D). Conversely, the use of the standard (Fig. 4, Panels B and E) and the distal POT (Fig. 4, Panels C and F) using both the nano crush and the DK crush approach allowed to obtain smaller areas of low WSS.

3.3. Baseline vs post-stenting geometry

Difference between the basal and post-stenting geometry obtained after virtual stent deployment are presented in Table 3. No significant differences were observed in the carina angle as well as in the areas (mm^2) of those regions of the geometry obtained after virtual stent deployment >0.25 mm from the baseline geometry.

4. Discussion

Our computational study, based on patient-specific coronary artery model and hemodynamic conditions, demonstrates a significant reduction in the mean WSS values in all the lesion's sites when the final POT was performed 1 mm distally the carina cut plane. Moreover, a significant improvement in the mean WSS values of the entire SB (e.g. LCX) was obtained performing the POT 1 mm distally to the carina cut plane. To the best of our knowledge, our study examined for the first time the hemodynamic impact, in terms of WSS, using different final POT positions in complex LM bifurcation disease.

Over the latest years, CFD analyses have been widely used in the field of coronary artery disease [27]. Moreover, the advent of patient-specific blood flow simulations has allowed to analyse the local rheological properties of stented regions further clarifying the device healing and other post-operative complications such as restenosis and thrombosis [8]. Several evidences have demonstrated that WSS plays a pivotal role in the neointimal formation and thrombosis. As result, WSS analyses can be translated into clinical practice improving interventional techniques and developing new stenting strategies [[28], [29], [30]].

The “ideal” POT currently represents a matter of discussion among interventional cardiologists worldwide. Indeed, the potential clinical impact of different POT positions to date remains unknown. Doubtless, from a hemodynamic viewpoint, the POT would be preferable over of kissing balloon inflation since the latter, as demonstrated by previous investigations, expands the stent asymmetrically resulting in lower and oscillatory WSS, thus increasing endothelial proliferation and the subsequent risk of in-stent restenosis (ISR) [[31], [32], [33]]. Conversely, the POT can expand the stent symmetrically in the bifurcation stent segments inducing a more homogenous strain distribution and a normal-high range of constant WSS at the luminal surface, which implies the induction of a neoathero-protective state maintaining the endothelial cells quiescent [8,34,35]. In our analysis, the need of performing a final POT in complex LM bifurcation stenting is unquestioned. However, our results seem to indicate that a distal POT could give some advantages in terms of WSS in the stented segments. A lower WSS values were observed in the proximal coronary artery regions, independently from the site in which the POT was performed. However, these values always were in the range of 1–7 Pa, which promotes a Neoathero-protective effect in stented segments [8,34,35].

The prevention of further coronary artery events must be based also on the existing interplay between WSS and some pro-inflammatory cytokines, such as tumor necrosis factor (TNF) and interleukin (IL)-1β, which are actively involved in the atherogenic pathways. Indeed, normal-high

WSS values, promotes a lower activation of endothelial cells due to the level of those cytokines [36,37].

A recent bench study on the mechanical benefits using different POT locations which have been defined as in our study, reported that the "distal" POT significantly overstretched the MV when compared to a POT performed just at the carina plan [38]. Unfortunately, this analysis did not provide any hemodynamic results and, hence, a comparison with our results is impossible.

Moreover, the significant normal-higher WSS values in the LCX represents an interesting finding since, as well known, the SB ostial restenosis and stent thrombosis remain areas where further improvements are needed [39].

No significant differences were observed comparing the baseline to the final post-stenting geometry. It is also true that to accurately assess this parameter, a post-operative imaging technique, able to reconstruct the coronary geometries should be used. However, as reported by Morlacchi et al., the post-operative geometry obtained after virtual stent deployment was rarely compared with the in vivo post-operative images [40]. In this regard, the improved WSS values observed in our study seems to be due to a more accurate post-dilation than to a distortion of the coronary artery geometry.

4.1. Study limitations

Our study presents some limitations. Firstly, the retrospective and monocentric design of the study. Secondly, the small number of patients evaluated. Since the outcome of CFD strictly depends on the quality of geometrical data, model reconstruction and boundary conditions, our methodology, based on the patient-specific 3D segmentation, reconstruction, stent implantation and subsequent fluid dynamic analysis, based on the patient-specific hemodynamic condition, allowing us to provide realistic models ad results. We excluded from the study those patients having other concomitant coronary lesions, which are frequently encountered in daily clinical practice since may have altered the results of CFD analysis. Doubtless, further refinements of the 3D reconstruction techniques for CFD simulations, using high-definition images from OCT allow to more accurately investigate the impact of stent design and strut thickness in vivo. Unfortunately, OCT is not available in our institution. Moreover, the concomitant use of IVUS, as fusion imaging technique with CCTA could have further improved the lumen reconstruction. However, the accuracy of CT-derived coronary lumen area in comparison to intravascular ultrasound has been validated in humans [41].

5. Conclusion

In patients with complex LM bifurcation disease the use of a final POT performed 1 mm distally to the carina cut plane might results in more favorable WSS patterns (i.e. higher WSS values) along all stented segments and, especially, along the entire LCX lesions. Our preliminary findings must be confirmed by further larger analyses performed both in-vitro and in-vivo, and by evaluating also geometrical and mechanical aspects, such as stent malapposition.

Author contributions

Conceptualization: Rigatelli G and Zuin M.

Methodology: Rigatelli G and Zuin M.

Software: Zuin M and Chiastra C.

Validation: Chiastra C.

Formal analysis: Rigatelli G and Zuin M.

Data curation: Rigatelli G.

Writing - original draft preparation: Rigatelli G and Zuin M.

Writing - review & editing: Rigatelli G and Chiastra C.

Supervision: Rigatelli G.

Declaration of competing interest

None of the authors have conflict of interest to declare.

References

[1]

A Hoye**The proximal optimisation technique for intervention of coronary bifurcations**
Interv Cardiol, 12 (2017), pp. 110-115
CrossRefView Record in ScopusGoogle Scholar

[2]

N Foin, GG Secco, L Ghilencea, R Krams, C Di Mario**Final proximal postdilatation is necessary after kissing balloon in bifurcation stenting**
EuroIntervention, 7 (2011), pp. 597-604
CrossRefView Record in ScopusGoogle Scholar

[3]

N Foin, A Mattesini, M Ghione, G Dall'ara, S Sen, S Nijjer, *et al.***Tools & techniques clinical: optimising stenting strategy in bifurcation lesions with insights from in vitro bifurcation models**
EuroIntervention, 9 (2013), pp. 885-887
CrossRefView Record in ScopusGoogle Scholar

[4]

P Guérin, P Pilet, G Finet, Y Gouëffic, JM N'Guyen, D Crochet, *et al.***Drug-eluting stents in bifurcations: bench study of strut deformation and coating lesions**
Circ Cardiovasc Interv, 3 (2010), pp. 120-126
View Record in ScopusGoogle Scholar

[5]

MW Basalus, KG van Houwelingen, MJ Ankone, J Feijen, C von Birgelen**Microcomputed tomographic assessment following extremely oversized partial postdilatation of drug-eluting stents**
EuroIntervention, 6 (2010), pp. 141-148
View Record in ScopusGoogle Scholar

[6]

JF Lassen, F Burzotta, AP Banning, T Lefèvre, O Darremont, D Hildick-Smith, *et al.***Percutaneous coronary intervention for the left main stem and other bifurcation lesions: 12th consensus document from the European Bifurcation Club**
EuroIntervention., 13 (2018), pp. 1540-1553
View Record in ScopusGoogle Scholar

[7]

G Rigatelli, M Zuin, K Karamfilof, D Cavazzini, G Braggion, S Perilli, *et al.***Impact of different final optimization techniques on long-term clinical outcomes of left main cross-over stenting**
Cardiovasc Revasc Med, 20 (2019), pp. 108-112
Article
Download PDFView Record in ScopusGoogle Scholar

[8]

F Gijsen, Y Katagiri, P Barlis, C Bourantas, C Collet, U Coskun, *et al.***Expert recommendations on the assessment of wall shear stress in human coronary arteries: existing methodologies, technical considerations, and clinical applications**
Eur Heart J, 40 (2019), pp. 3421-3433
CrossRefView Record in ScopusGoogle Scholar

[9]

M Zuin, G Rigatelli, D Vassilev, F Ronco, A Rigatelli, L Roncon**Computational fluid dynamic-derived wall shear stress of non-significant left main bifurcation disease may predict acute vessel thrombosis at 3-year follow-up**
Heart Vessels, 35 (2020), pp. 297-306
CrossRefView Record in ScopusGoogle Scholar

[10]

A Medina, J Suarez de Lezo, M Pan**A new classification of coronary bifurcation lesions**
Rev Esp Cardiol, 59 (2006), p. 183
Article
Download PDFCrossRefView Record in ScopusGoogle Scholar

[11]

G Holzapfel, G Sommer, CT Gasser, P Regitnig**Determination of layer-specific mechanical properties of human coronary arteries with nonatherosclerotic intimal thickening and related constitutive modeling**
Am J Physiol Heart Circ Physiol, 289 (2005), pp. H2048-H2058
CrossRefView Record in ScopusGoogle Scholar

[12]

HM Loree, AJ Grodzinsky, SY Park, LJ Gibson, RT Lee**Static circumferential tangential modulus of human atherosclerotic tissue**
J Biomech, 27 (1994), pp. 195-204
Article
Download PDFView Record in ScopusGoogle Scholar

[13]

GC Cheng, HM Loree, RD Kamm, MC Fishbein, RT Lee**Distribution of circumferential stress in ruptured and stable atherosclerotic lesions. A structural analysis with histopathological correlation**
Circulation., 87 (1993), pp. 1179-1187
View Record in ScopusGoogle Scholar

[14]

M Dominici, A Arrivi, M Bazzucchi, M De Paolis, C Milici, C Bock, *et al.***Effectiveness of novel stent platform eluting sirolimus from a biodegradable polymer in percutaneous coronary intervention**
Minerva Cardioangiol, 64 (2016), pp. 1-8
View Record in ScopusGoogle Scholar

[15]

W Schmidt, P Lanzer, P Behrens, C Brandt-Wunderlich, A Öner, H Ince, *et al.***Direct comparison of coronary bare metal vs. drug-eluting stents: same platform, different mechanics?**

Eur J Med Res, 23 (2) (2018)
Google Scholar

[16]

G Rigatelli, M Zuin, F Dell'Avvocata, D Vassilev, R Daggubati, T Nguyen, *et al.***Complex coronary bifurcation treatment by a novel stenting technique: bench test, fluid dynamic study and clinical outcomes**
Catheter Cardiovasc Interv, 92 (2018), pp. 907-914
CrossRefView Record in ScopusGoogle Scholar

[17]

SL Chen, JJ Zhang, Y Han, J Kan, L Chen, C Qiu, *et al.***Double kissing crush versus provisional stenting for left main distal bifurcation lesions: DKCRUSH-V randomized trial**
J Am Coll Cardiol, 70 (2017), pp. 2605-2617
Article
Download PDFView Record in ScopusGoogle Scholar

[18]

M De Beulea, P Mortier, SG Carlierc, B Verhegged, R Van Impera, P Verdonckb**Realistic finite element based stent design: the impact of balloon folding**
J Biomech, 41 (2008), pp. 383-389
Google Scholar

[19]

F Gervaso, C Capelli, L Petrini, S Lattanzio, L Di Virgilio, F Migliavacca**On the effects of different strategies in modelling balloon-expandable stenting by means of finite element method**
J Biomech, 41 (2008), pp. 1206-1212
Article
Download PDFView Record in ScopusGoogle Scholar

[20]

S Morlacchi, SG Colleoni, R Cárdenes, C Chiastra, JL Diez, I Larrabide, *et al.***Patient-specific simulations of stenting procedures in coronary bifurcations: two clinical cases**
Med Eng Phys, 35 (2013), pp. 1272-1281
Article
Download PDFView Record in ScopusGoogle Scholar

[21]

C Chiastra, S Morlacchi, S Pereira, G Dubinia, F Migliavacca**Computational fluid dynamics of stented coronary bifurcations studied with a hybrid discretization method**
Eur J Mech B Fluids, 35 (2012), pp. 76-84
Article
Download PDFView Record in ScopusGoogle Scholar

[22]

G Rigatelli, F Dell'Avvocata, M Zuin, S Giatti, K Duong, T Pham, *et al.***Comparative computed flow dynamic analysis of different optimization techniques in left main either provisional or culotte stenting**

J Transl Int Med, 5 (2017), pp. 205-212

CrossRefView Record in ScopusGoogle Scholar

[23]

G Rigatelli, M Zuin, F Dell'Avvocata, D Vassilev, R Daggubati, T Nguyen, *et al.***Evaluation of coronary flow conditions in complex coronary artery bifurcations stenting using computational fluid dynamics: impact of final proximal optimization technique on different double-stent techniques**

Cardiovasc Revasc Med, 18 (2017), pp. 233-240

Article

Download PDFView Record in ScopusGoogle Scholar

[24]

A Theodorakakos, M Gavaises, A Andriotis, A Zifan, P Liatsis, I Pantos, *et al.***Simulation of cardiac motion on non-Newtonian, pulsating flow development in the human left anterior descending coronary artery**

Phys Med Biol, 53 (2008), pp. 4875-4879

CrossRefView Record in ScopusGoogle Scholar

[25]

S Shibeshi, W Collins**The rheology of blood flow in a branched arterial system**

Appl Rheol, 15 (2005), pp. 398-405

CrossRefView Record in ScopusGoogle Scholar

[26]

CD Murray**The physiological principle of minimum work. The vascular system and the cost of blood volume**

Proc. Natl. Acad. Sci, 12 (1926), pp. 207-214

CrossRefView Record in ScopusGoogle Scholar

[27]

M Zuin, G Rigatelli, G Faggian, RL Mathematics**Cardiovascular interventions: role of the finite element modeling in clinical decision making**

JACC Cardiovasc Interv, 9 (2016), pp. 507-508

Article

Download PDFView Record in ScopusGoogle Scholar

[28]

C Chiastra, S Migliori, F Burzotta, G Dubini, F Migliavacca**Patient-specific modeling of stented coronary arteries reconstructed from optical coherence tomography: towards a widespread clinical use of fluid dynamics analyses**
J Cardiovasc Transl Res, 11 (2018), pp. 156-172
CrossRefView Record in ScopusGoogle Scholar

[29]

AP Antoniadis, P Mortier, G Kassab, G Dubini, N Foin, Y Murasato, *et al.***Biomechanical modeling to improve coronary artery bifurcation stenting: expert review document on techniques and clinical implementation**
JACC Cardiovasc Interv, 8 (2015), pp. 1281-1296
Article
Download PDFView Record in ScopusGoogle Scholar

[30]

F Migliavacca, C Chiastra, YS Chatzizisis, G Dubini**Virtual bench testing to study coronary bifurcation stenting**
EuroIntervention, 11 (Suppl V) (2015), pp. V31-V34
CrossRefView Record in ScopusGoogle Scholar

[31]

S Morlacchi, C Chiastra, D Gastaldi, G Pennati, G Dubini, F Migliavacca**Sequential structural and fluid dynamic numerical simulations of a stented bifurcated coronary artery**
J Biomech Eng, 133 (2011), pp. 121010-121011
View Record in ScopusGoogle Scholar

[32]

D Hakim, A Chatterjee, O Alli, J Turner, A Sattar, N Foin, *et al.***Role of proximal optimization technique guided by intravascular ultrasound on stent expansion, stent symmetry index, and side-branch hemodynamics in patients with coronary bifurcation lesions**
Circ Cardiovasc Interv, 10 (2017), Article e005535
CrossRefView Record in ScopusGoogle Scholar

[33]

M Sanmartín, J Goicolea, C García, J García, A Crespo, J Rodríguez, *et al.***Influence of shear stress on in-stent restenosis**
Rev Esp Cardiol, 59 (2006), pp. 20-27
Article
Download PDFCrossRefView Record in ScopusGoogle Scholar

[34]

K Van der Heiden, FJ Gijsen, A Narracott, S Hsiao, I Halliday, J Gunn, *et al.***The effects of stenting on shear stress: relevance to endothelial injury and repair**

Cardiovasc Res, 99 (2013), pp. 269-275
CrossRefView Record in ScopusGoogle Scholar

[35]

R Torii, E Tenekecioglu, C Bourantas, E Poon, V Thondapu, F Gijsen, *et al.***Five-year follow-up of underexpanded and overexpanded bioresorbable scaffolds: self-correction and impact on shear stress**
EuroIntervention, 12 (2017), pp. 2158-2159
CrossRefView Record in ScopusGoogle Scholar

[36]

JJ Chiu, PL Lee, CN Chen, CI Lee, SF Chang, LJ Chen, *et al.***Shear stress increases ICAM-1 and decreases VCAM-1 and E-selectin expressions induced by tumor necrosis factor-alpha in endothelial cells**
Arterioscler Thromb Vasc Biol, 24 (2004), pp. 73-79
View Record in ScopusGoogle Scholar

[37]

J Partridge, H Carlsen, K Enesa, H Chaudhury, M Zakkar, L Luong, *et al.***Laminar shear stress acts as a switch to regulate divergent functions of NF-kappa B in endothelial cells**
FASEB J, 21 (2007), pp. 3553-3561
CrossRefView Record in ScopusGoogle Scholar

[38]

F Dérimay, G Rioufol, T Nishi, Y Kobayashi, WF Fearon, J Veziers, *et al.***Optimal balloon positioning for the proximal optimization technique? An experimental bench study**
Int J Cardiol, 292 (2019), pp. 95-97
Article
Download PDFView Record in ScopusGoogle Scholar

[39]

I Narbute, S Jegere, I Kumsars, D Juhnevica, A Knipse, A Erglis**Real-life bifurcation — challenges and potential complications**
Interventional Cardiology Review, 7 (2012), pp. 95-99
CrossRefView Record in ScopusGoogle Scholar

[40]

S Morlacchi, SG Colleoni, R Cárdenes, C Chiastra, JL Diez, I Larrabide, *et al.***Patient-specific simulations of stenting procedures in coronary bifurcations: two clinical cases**
Med Eng Phys, 35 (2013), pp. 1272-1281
Article
Download PDFView Record in ScopusGoogle Scholar

[41]

PK Siogkas, MI Papafaklis, AI Sakellarios, KA Stefanou, CV Bourantas, LS Athanasiou, *et al.***Patient-specifc simulation of coronary artery pressure measurements: an in vivo three-dimensional validation study in humans**

Biomed Res Int, 2015 (2015), p. 628416

View Record in ScopusGoogle Scholar

Table 1. Baseline coronary artery derived measurements. LM: Left main; LAD: Left anterior descending; LCX: Left circumflex; DS: 3-diemnsional percentage of diameter stenosis.

	N=8
LM lesion length, mm	0.85±0.11
LAD lesion length, mm	0.79±0.16
LCX lesion length, mm	0.76±0.13
DS LM (%)	72.1±11.2
DS LAD (%)	67,3±14.3
DS LCX (%)	70.7±12.8
Carena Angle, °	72.3±18.6

Table 2. Mean wall shear stress after final POT according to the site and the technique.

	Distal POT N=8	Current POT N=8	Proximal POT N=8	P ANOVA
		Nano Crush		
LM				
WSS_{prox} (Pa)	6.2±0.2 °	5.4±0.6 *	3.2±0.4	<0.001
WSS_{med} (Pa)	6.4±0.7	6.0±0.2 *	3.3±0.4	<0.001
WSS_{distal} (Pa)	6.5±0.2°°	5.8±0.5 *	3.5±0.2	<0.001
$LM_{(entire\_lesion)}$ (Pa)	6.3±0.4	5.7±0.7 *	3.3±0.3	<0.001
LAD WSS				
WSS_{prox} (Pa)	6,1±0.6	6.0±0.2 *	4.3±0.6	0.02
WSS_{med} (Pa)	6.3±0.5	5.8±0.5 *	3.6±0.4	<0.001
WSS_{distal} (Pa)	6.0±0.8	5.8±0.2 *	3.4±07	0.03
$LAD_{(entire\_lesion)}$ (Pa)	6.1±0.6	5.9±0.3 *	3.7±0.5	<0.001
LCX WSS				
WSS_{prox} (Pa)	6.2±0.6	5.9.±0.5 *	3.9±0.2	0.001
WSS_{med} (Pa)	6.1±0.5	5.5±0.9 *	3.8±0.3	0.003
WSS_{distal} (Pa)	6.1±0.1 #	5.2±0.8 *	3.5±0.3	<0.001
$LCX_{(entire\_lesion)}$ (Pa)	6.1±0.2 ##	5.5±0.7 *	3.7±0.2	0.001
		DK crush		
LM				
WSS_{prox} (Pa)	6.1±0.3°	5.6±0.4 *	3.3±0.6	<0.001
WSS_{med} (Pa)	6.2±0.5	6.2±0.4 *	3.3±0.8	0.002
WSS_{distal} (Pa)	6.3±0.4	5.9±0.6 *	3.7±0.4	0.003

$LM_{(entire\_lesion)}$ (Pa)	6.2±0.6	5.9±0.3 *	3.4±0.5	0.001
LAD WSS				
WSS_{prox} (Pa)	6.0±0.5	6.2±0.4 *	4.5±0.3	0.001
WSS_{med} (Pa)	6.3±0.6	5.6±0.7 *	3.9±0.2	<0.001
WSS_{distal} (Pa)	6.2±0.6°°	5.6±0.5 *	3.6±0.4	<0.001
$LAD_{(entire\_lesion)}$ (Pa)	6.2±0.6	5.8±0.3 *	4.0±0.3	0.003
LCX WSS				
WSS_{prox} (Pa)	6.3±0.8	5.7±0.8 *	3.8±0.4	0.001
WSS_{med} (Pa)	6.2±0.4	5.9±0.5 *	3.6±0.2	0.002
WSS_{distal} (Pa)	6.1±0.4 #	5.3±0.5 *	3.5±0.5	<0.001
$LCX_{(entire\_lesion)}$ (Pa)	6.2±0.6 ##	5.6±0.6 *	3.6±0.3	0.001

For the Nano crush: °p=0.003, °°p=0.002, #p=0.007 and ## p=0.03 between distal and current POT; *p<0.001 between current and proximal POT for all items.

For the DK crush: °p=0.01, p=0.04, #p=0.003 and ##p=0.02 between distal and current POT: *p<0.001 between current and proximal POT for all items.

Figures.

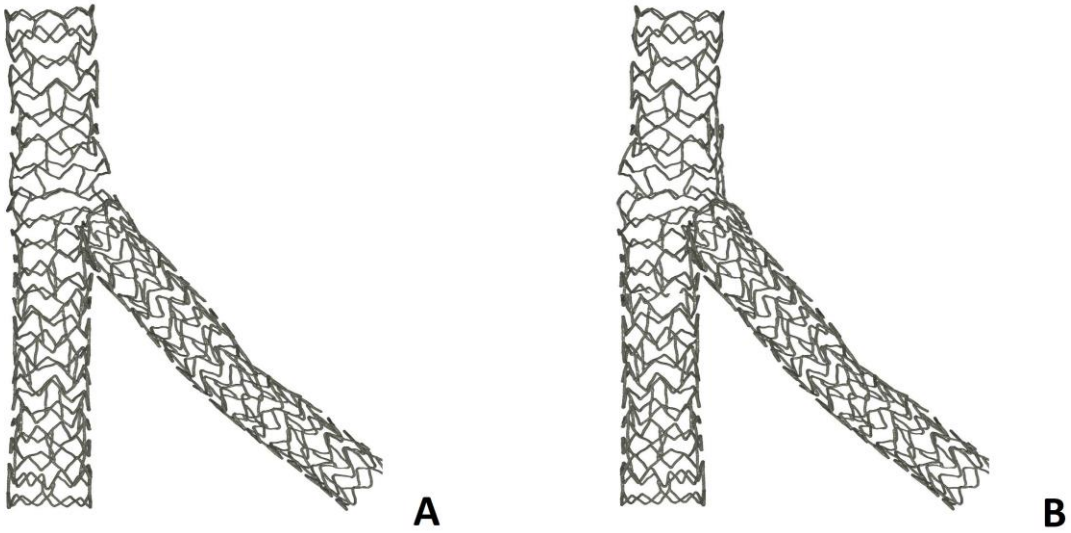

Figure 1. 3D reconstruction of the stent structure using the Nano crush (A) and DK crush (B) techniques after the virtual implantation.

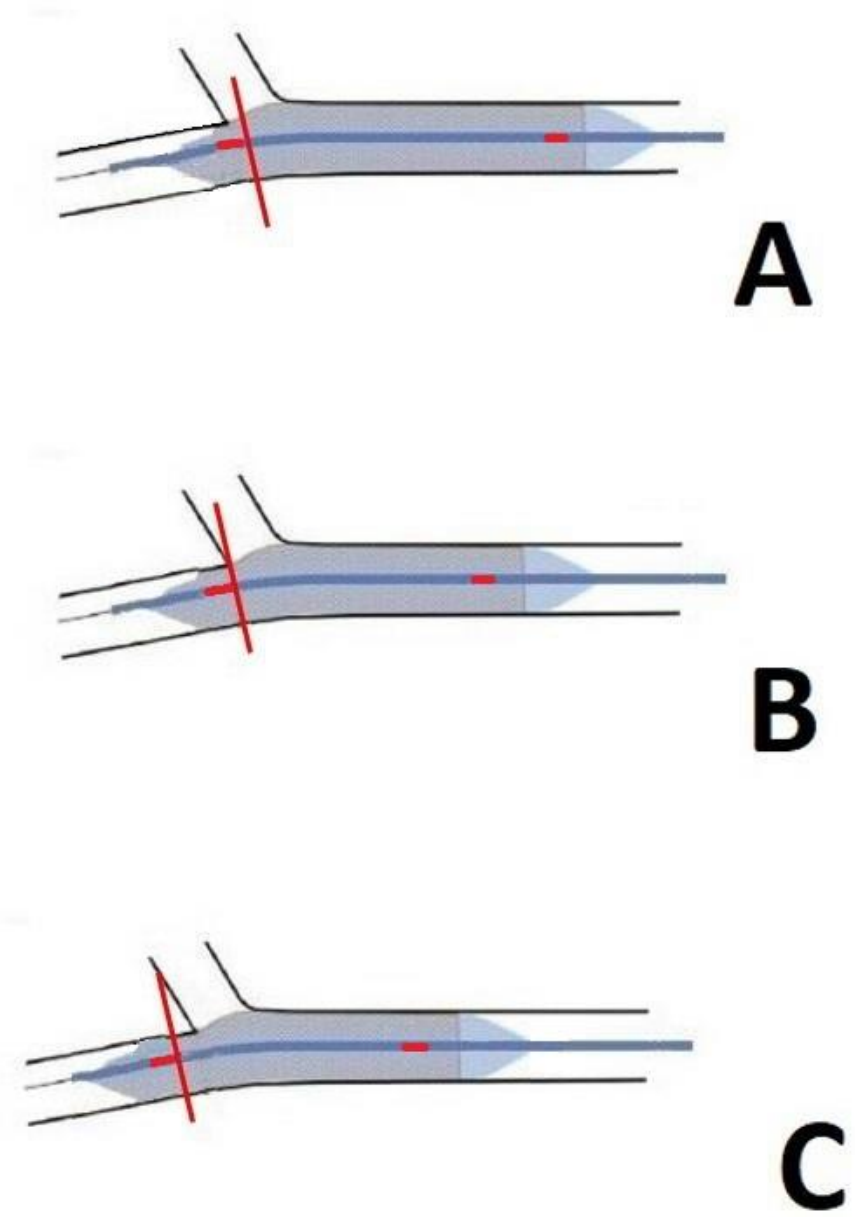

Figure 2. Schematic representation illustrating the different post optimization technique (POT) balloon positioning in the left main, defined as proximal, defined as 1 mm before the carina cut plane (A), current, defined as just at the carina cut plane (B) and distal, defined as 1 mm after the carina cut plane (C).

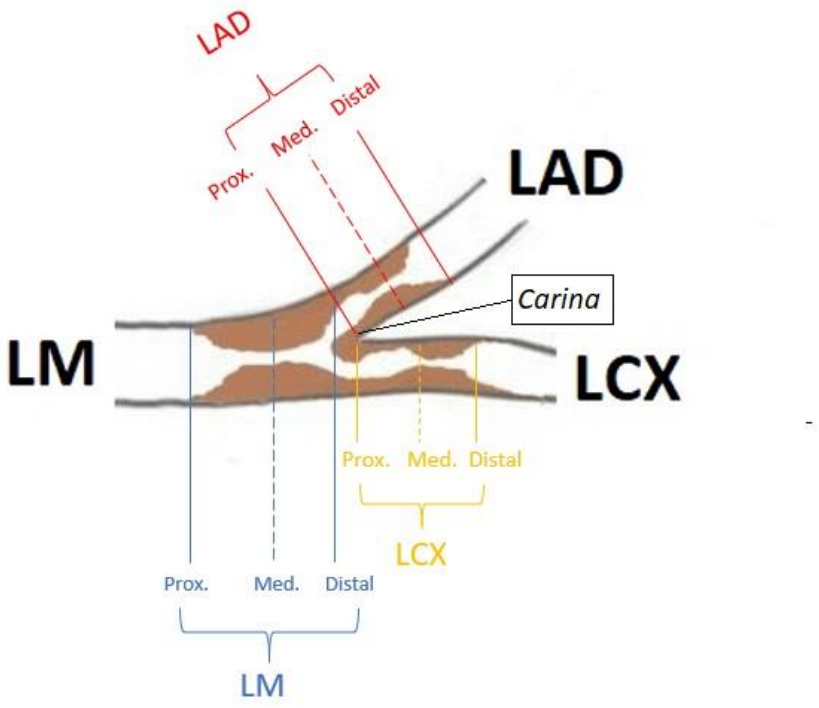

Figure 3. Schematic representation of the left main bifurcation partition. Coronary computed tomography angiography images were used to segment and reconstruct the coronary artery bifurcation. To create segment-specific wall shear stress (WSS) values each vessel was divided into three segments defined a s proximal (Prox.), medial (Med.) and distal (Distal) (see the text for the explanation). LM: Left main; LAD; left anterior descending.

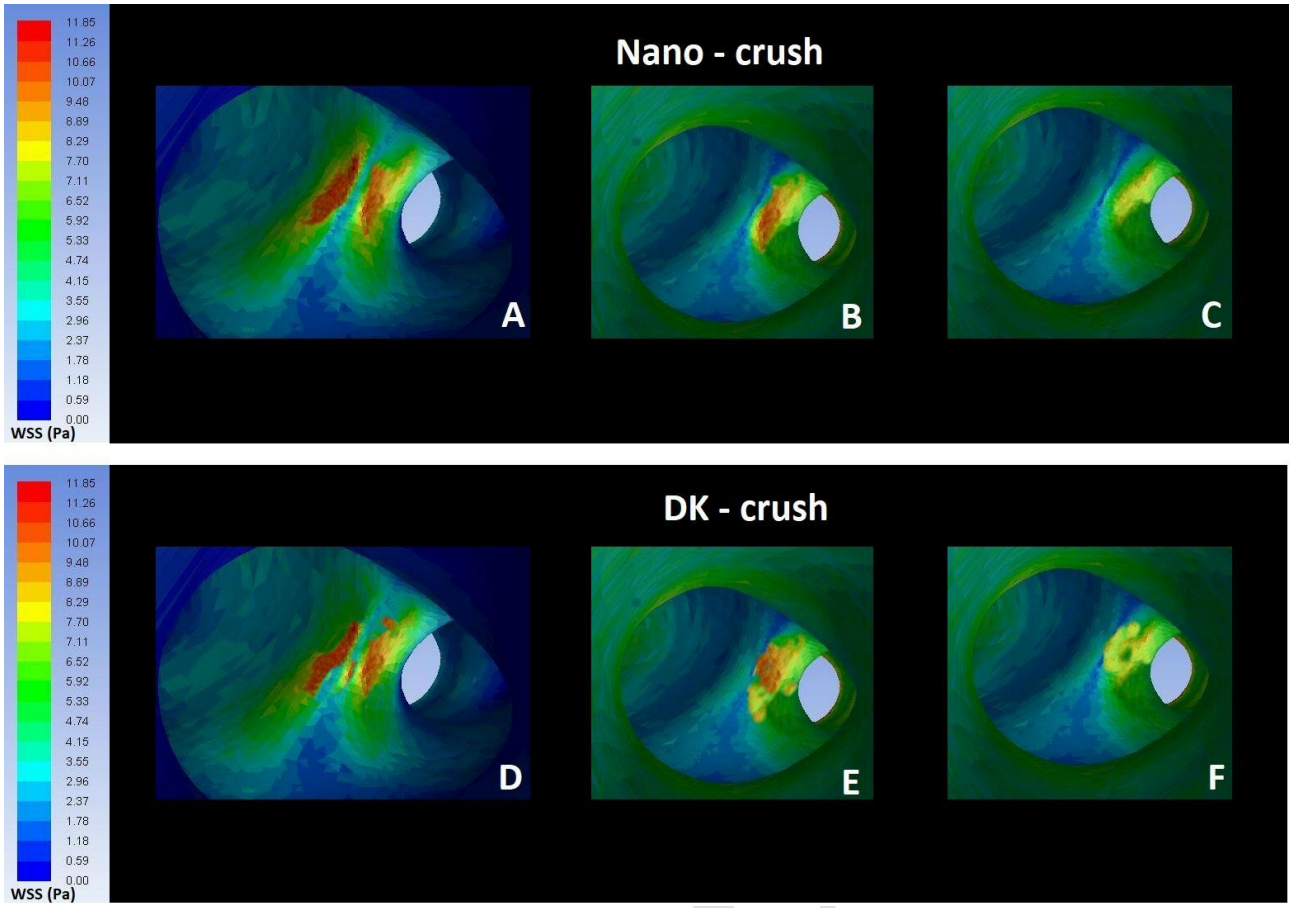

Figure 4. Comparison of the mean wall shear stress (WSS) values observed at the carina inside the bifurcated vessel. Proximal (A), current (B) and distal (C) post optimization technique using the Nano crush. Proximal (D), current (E) and distal (F) post optimization technique using the DK crush. The stent has been removed to clearly show the different WSS contours along the vascular segments of interest.